Optics & Laser Technology 71 (2015) 108–113

Contents lists available at ScienceDirect

Optics & Laser Technology

journal homepage: www.elsevier.com/locate/optlastec

Growth and characterization of a new organic nonlinear optical crystal: 1-(3-Nitrophenyl)-5-phenylpenta-2,4-dien-1-one

P.S. Patil [a,*], P. Ajay Kumar [b], S. Venugopal Rao [b], G. Bhagavannarayana [c]

[a] Department of Physics, K. L. E. Institute of Technology, Opposite Airport, Gokul, Hubli 580030, India
[b] Advanced Centre of Research in High Energy Materials (ACRHEM), University of Hyderabad, Hyderabad 500046, India
[c] Crystal Growth & X-ray Analysis, CSIR-National Physical Laboratory, New Delhi 110012, India

ARTICLE INFO

Article history:
Received 24 January 2015
Accepted 5 March 2015

Keywords:
Organic compounds
Nonlinear optical material
Two-photon absorption

ABSTRACT

Organic nonlinear optical single crystal of 1-(3-Nitrophenyl)-5-phenylpenta-2,4-dien-1-one (Ci3NC) with dimensions $25 \times 15 \times 10$ mm^3 was successfully grown for the first time by the slow evaporation solution growth technique (SEST). The structural perfection of the grown crystals has been analyzed by high-resolution X-ray diffraction (HRXRD) rocking curve measurements, and it was found that the crystalline perfection is reasonably good having very low angle (tilt angle $\leq 1'$) internal structural grain boundary. Thermo-gravimetric analysis (TGA) and differential thermal analysis (DTA) were used to study its thermal properties. Powder test with Nd:YAG laser radiation shows second harmonic generation which is about 7 times that of urea. The optical transmittance window and the lower cutoff wavelength of the Ci3NC have been identified by UV–vis–NIR studies. Third-order nonlinear optical (NLO) response of Ci3NC has been examined using Z-scan technique with femtosecond (fs), MHz pulses at wavelengths of 870 nm and 900 nm. Various NLO coefficients such as two-photon absorption (2PA) coefficient (β), three photon absorption (3PA) coefficient (γ), and nonlinear refractive index (η_2) were evaluated.

1. Introduction

The current optoelectronics industry is highly motivated to discover new nonlinear optical (NLO) materials since they are vital for advanced display technologies, telecommunications and the laser industry [1]. Specifically, NLO materials are key sources of red, green and blue light for RGB displays and laser application, on account of their ability to act as wavelength converter. Different types of molecular and bulk materials have been examined for nonlinear optical properties [2]. Organic nonlinear materials are attracting a great deal of attention, as they have large optical susceptibilities, inherent ultrafast response times, and high optical thresholds for laser power as compared with inorganic materials [2,3]. Organic molecules with significant nonlinear optical activity generally consist of a π-electron conjugated structure. The conjugated π-electron moiety provides a pathway for the entire length of conjugation under the perturbation of an external electric field. Fictionalization of both ends of the π-bond systems with appropriate electron donor and acceptor group can increase the asymmetric electronic distribution in either or both the ground and excited states, thus leading to an increased optical nonlinearity [4–7].

In view of the importance of organic nonlinear materials and also as a part of our ongoing work [8–10], the investigation of growth and characterization of 1-(3-Nitrophenyl)-5-phenylpenta-2,4-dien-1-one (Ci3NC) is undertaken. We have already reported synthesis and single crystal structure of Ci3NC [11]. Ci3NC ($C_{17}H_{13}NO_3$, Mr=279.28) crystallizes in the orthorhombic space group $P2_12_12_1$ with lattice parameters $a=7.0167$ (1) Å, $b=12.1953$ (2) Å, $c=16.1081$ (3) Å and there are four molecules per unit cell [11]. As a part of extensive characterization, we present in this article, the investigation of the crystal growth, transmission cutoff, the SHG efficiency, nonlinear absorption and refraction, thermal expansion and HRXRD of this material.

2. Experimental procedure

2.1. Material synthesis

The general synthetic strategy employed to prepare 1-(3-Nitrophenyl)-5-phenylpenta-2,4-dien-1-one was based on Claisen–Schmidt condensation, which has been previously reported [11]. The chemical structure of Ci3NC and the schematic representation of the reaction is given in Scheme 1.

* Corresponding author. Fax: +91 836 2330688.
E-mail address: pspatilcrystal@gmail.com (P.S. Patil).

http://dx.doi.org/10.1016/j.optlastec.2015.03.002
0030-3992/

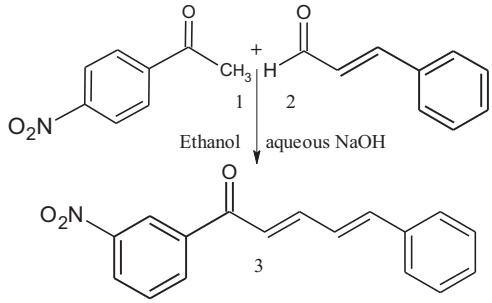

Scheme 1. Chemical structure (3) and synthesis scheme of 1-(3-Nitrophenyl)-5-phenylpenta-2,4-dien-1-one.

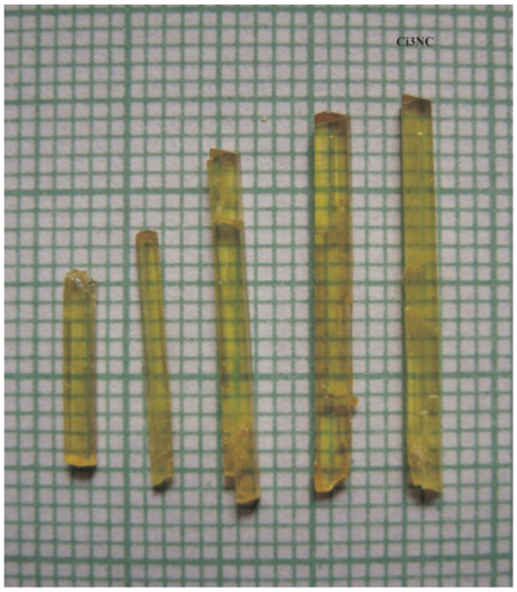

Fig. 1. Photograph of as grown Ci3NC crystals.

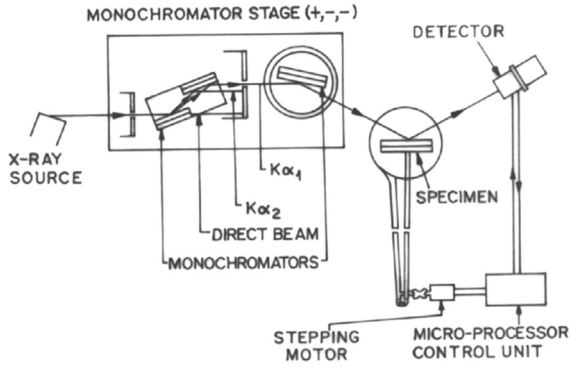

Fig. 2. Schematic line diagram of the multi-crystal X-ray diffractometer.

2.2. Crystal growth

Large sized good quality single crystals are essential to evaluate their physical properties reliably. Selection of suitable solvent and optimization of growth conditions are crucial for this purpose. It was found that Ci3NC was insoluble in water, moderately soluble in acetone and highly soluble in dimethylformamide (DMF). The solution of the growth material was prepared in DMF. After filtration by using Whatman filter paper, the solution was transferred into a crystal growth vessel. Next, it was kept for crystallization by slow evaporation at room temperature (30 °C). At the period of super saturation, tiny crystals were nucleated. They were allowed to grow to maximum possible dimensions and then harvested. Transparent thick needles like crystals appeared in the growth vessels within 15 days of solution evaporation. Fig. 1 shows the photograph of as grown crystals. The crystals obtained are nonhygroscopic, stable at room temperature and exhibit a needle like shape. The needle-like structure of the crystal is considered to play an active role in the second harmonic process [12].

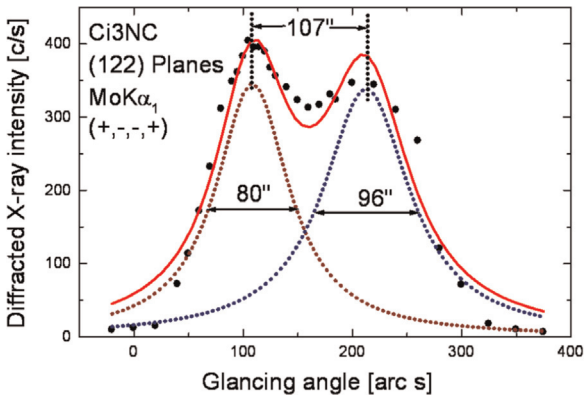

Fig. 3. Diffraction curve recorded for Ci3NC single crystal for (122) diffracting planes by employing the multi-crystal X-ray diffractometer with MoKα_1 radiation.

2.3. Characterization

To reveal the crystalline perfection of the grown crystals, a multi-crystal X-ray diffractometer (MCD) developed at NPL [13] has been used to record high-resolution diffraction curves (DCs). Fig. 2 shows the schematic diagram of the multi-crystal X-ray diffractometer. In this system a fine focus (0.4×8 mm^2; 2 kW Mo) X-ray source energized by a well-stabilized Philips X-ray generator (PW 1743) was employed. The well-collimated and monochromatic MoKα_1 beam obtained from the three monochromator (111) Si crystals set in dispersive $(+,-,-)$ configuration has been used as the exploring X-ray beam. This arrangement improves the spectral purity ($\Delta\lambda/\lambda \ll 10^{-5}$) of the MoK$\alpha_1$ beam. The divergence of the exploring beam in the horizontal plane (plane of diffraction) was estimated to be $\ll 3''$. The specimen crystal is aligned in the $(+,-,-,+)$ configuration. Due to dispersive configuration, though the lattice constant of the monochromator crystal(s) and the specimen are different, the unwanted dispersion broadening in the diffraction curve of the specimen crystal is insignificant. The specimen can be rotated about a vertical axis, which is perpendicular to the plane of diffraction, with minimum angular interval of $0.5''$. The diffracted intensity is measured by using an in-house developed scintillation counter. To provide two-theta ($2\theta_B$) angular rotation to the detector (scintillation counter) corresponding to the Bragg diffraction angle (θ_B), it is coupled to the radial arm of the goniometer of the specimen stage. The rocking or diffraction curves were recorded by changing the glancing angle (angle between the incident X-ray beam and the surface of the specimen) around the Bragg diffraction peak position θ_B starting from a suitable arbitrary glancing angle. The detector was kept at the same angular position $2\theta_B$ with wide opening for its slit, the so-called ω scan.

For the optical transmission study, the UV–vis NIR spectra were recorded in the range of 300–1100 nm using Shimadzu UV-1061 UV–vis spectrophotometer. The spectra were recorded for DMF solution of Ci3NC in a quartz cell of 10 mm length. Differential thermal analysis (DTA) and thermogravimetric analysis (TGA) of the Ci3NC crystals were carried out using the Shimadzu DT-40 simultaneous DTA/TGA analyzer with a heating rate of 10 °C/min.

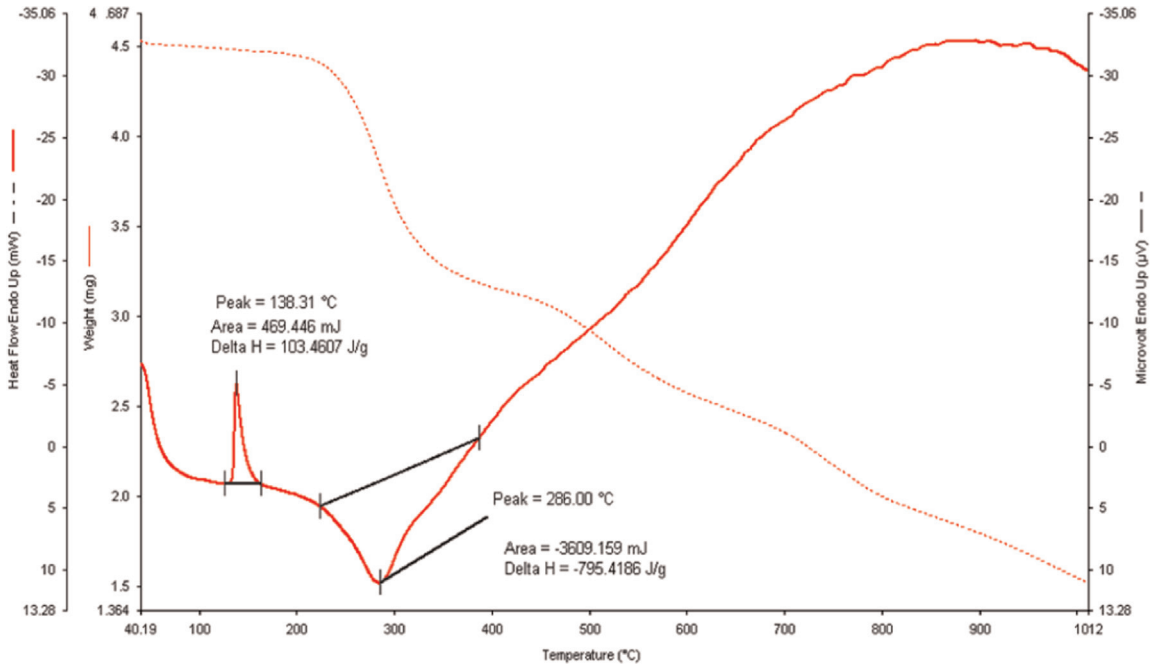

Fig. 4. TGA and DTA curves of Ci3NC.

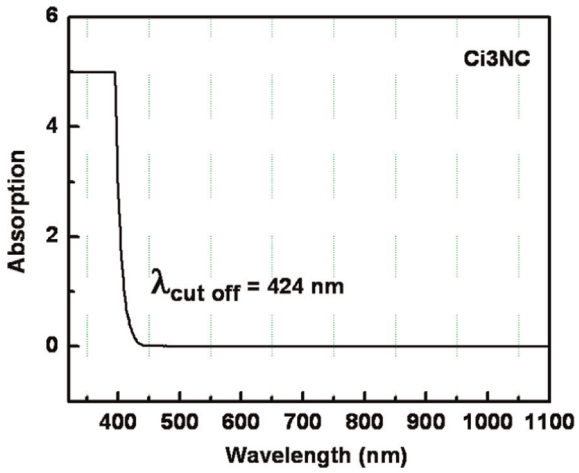

Fig. 5. UV–vis NIR absorption spectra of Ci3NC.

A preliminary study of the powder SHG conversion efficiency was carried according to a method developed by Kurtz and Perry [14]. A Q-switched Nd:YAG laser beam (of wavelength 1064 nm with an input power of 8 mJ, and a pulse width of 8 ns with a repetition rate of 10 Hz) was incident normally on the sample capillary tube and the output from the sample was passed through a monochromator to collect the intensity of 532 nm component. The generation of second harmonic was confirmed by the emission of green light. The fundamental wave was eliminated by passing the beam through filter consisting of $CuSO_4$ solution, which absorbed the 1064 nm light. Another filter BG-38 also removed any residual 1064 nm light. Second harmonic radiation generated by the randomly oriented micro-crystals (of particle size less than 60 mm) was focused by a lens. The amplitude of the SHG output voltage was measured using photomultiplier and digitalizing oscilloscope assembly. The second harmonic (SH) signal was converted into electrical signal using a photomultiplier tube and was finally displayed on a digital storage oscilloscope. Similar procedure was employed to measure the amplitude of reference material urea, which was powdered to the identical particle size and taken in a capillary.

Third-order NLO characterization was accomplished using the standard Z-scan technique [15,19–21]. In the fs regime, fs pulses were delivered by a Ti:sapphire oscillator (repetition rate ~80 MHz, pulse duration ~150 fs, total average power of ~4 W). The Z-scan experiments were performed with typically 20–30 mW input power with corresponding pulse energy being ~50 nJ. The pulses were tunable in the wavelength region of 680–1060 nm. The sample was scanned along the *Z*-direction through the focus of the beam passed through a 100 mm focal length lens. The input beam was spatially filtered to attain a pure Gaussian profile in the far field. The sample was placed on a 10 µm resolution translation stage and data was collected manually using a power meter detector (Field-Max). The transmitted intensity was recorded as a function of the sample position. The beam waist (ω_o) estimated at the focus was ~25 µm with a corresponding Rayleigh range of ~2.26 mm. Initially closed aperture scans were performed at intensities where the contribution from the higher order nonlinear effects is negligible (the value of $\Delta\phi$ estimated in all the cases was found to be $<\pi$). In addition, nonlinear refraction and absorption measurements were also performed for two different chopper frequencies 1 kHz and 500 Hz by placing an optical chopper in the experimental setup. The experiments were performed at two wavelengths of 870 nm and 900 nm.

3. Results and discussion

3.1. Multi-crystal X-ray diffractometer

Fig. 3 shows the high-resolution diffraction curve (DC) recorded for Ci3NC specimen crystal using (122) diffracting planes in symmetrical Bragg geometry by employing the multi-crystal X-ray diffractometer described above with $MoK\alpha_1$ radiation. As seen in the figure, the curve is not having a single diffraction peak. The solid line, which follows well with the experimental points (filled circles), is the convoluted curve of two peaks using the Lorentzian fit. The additional peak depicts an internal structural low angle

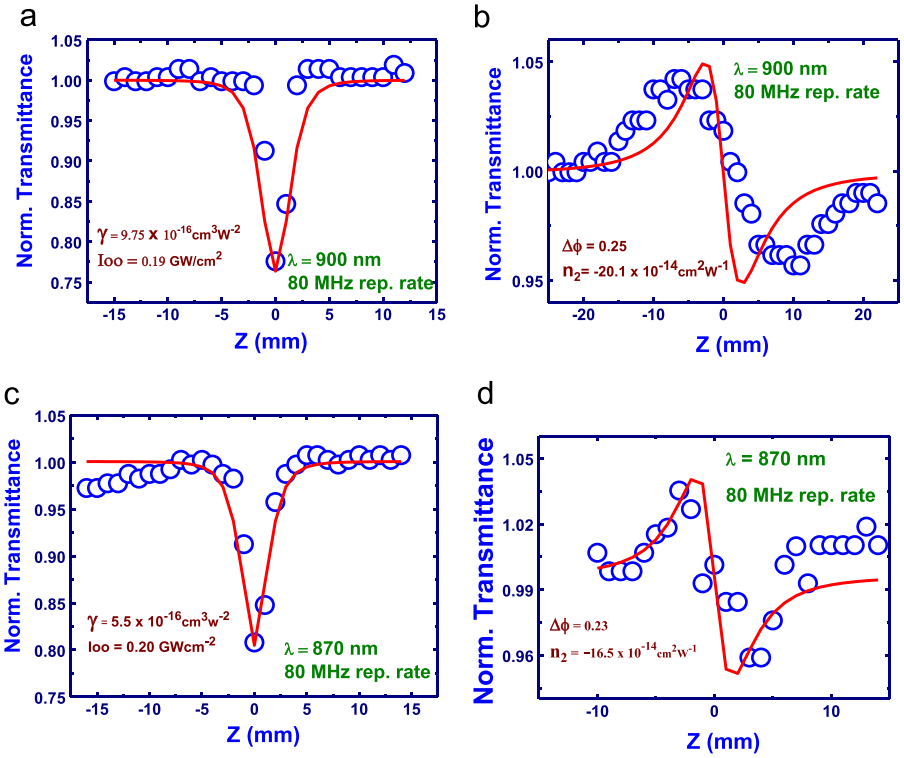

Fig.6. The recorded open aperture and closed aperture Z-scan traces of Ci3NC at 80 MHz.(a) and (b) represent 900 nm Z-scan data. (c) and (d) represent 870 nm Z-scan data. The circles are the experimental data and solid lines are the corresponding theoretical fits.

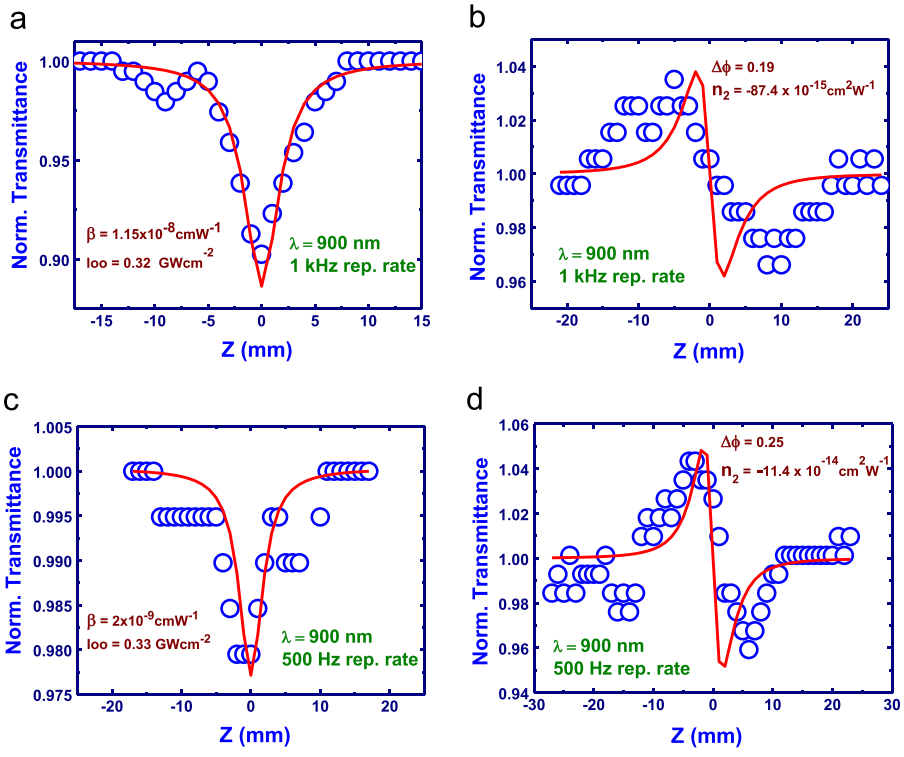

Fig.7. The recorded open aperture and closed aperture Z-scan traces of Ci3NC using a chopper. (a) and (b) represent 900 nm Z-scan data at 1 kHz. (c) and (d) represent 900 nm Z-scan data at 500 Hz. The circles are the experimental data and solid lines are the corresponding theoretical fits.

(tilt angle $>1'$ but less than an arc degree) boundary [16] whose tilt angle (misorientation angle between the two crystalline regions on both sides of the structural grain boundary) is $107''$ from its adjoining region. The full width at half maximum (FWHM) of the main peak and the very low angle boundary are respectively $80''$ and $96''$. Though the specimen contains a low angle boundary, the relatively low angular spread of around $400''$ of the diffraction curve and the low FWHM values show that the crystalline perfection is reasonably good. The entrapment of impurities or solvent molecules could be responsible for the formation of these

Table 1
Measured 2PA coefficient (β), 3PA coefficient (γ), and nonlinear refractive index (n_2) for Ci3NC in DMF solutions with a concentration of 5 mM at wavelengths of 870 nm and 900 nm.

Wavelength (λ) (nm)	Rep. rate	β (cm W^{-1})	γ (cm^3 W^{-2})	n_2 (cm^2 W^{-1})	Re $\chi^{(3)}$ e.s.u.	Im $\chi^{(3)}$ e.s.u.	$\chi^{(3)}$ e.s.u.
900	500 Hz	2.0×10^{-9}	–	-11.4×10^{-14}	0.89×10^{-11}	0.11×10^{-11}	0.90×10^{-11}
900	1 kHz	1.15×10^{-8}	–	-87.4×10^{-15}	0.68×10^{-11}	0.64×10^{-11}	0.93×10^{-11}
870	80 MHz	–	5.5×10^{-16}	-16.5×10^{-14}	1.29×10^{-11}	–	–
900	80 MHz	–	9.8×10^{-16}	-20.1×10^{-14}	1.56×10^{-11}	–	–

grain boundaries which may be segregated at the boundaries during the growth process. It may be mentioned here that such a low angle boundary could be detected with well-resolved peak in the diffraction curve only because of the high-resolution of the multi-crystal X-ray diffractometer used in the present studies. The influence of such minute defects on the NLO properties is very insignificant. However, a quantitative analysis of such unavoidable defects is of great importance, particularly in the case of phase matching applications.

3.2. Thermal studies

The results of TG/DTA analysis are shown in Fig. 4. The DTA curve implies that the material undergoes an irreversible endothermic peak at temperature 138.31 °C, corresponding to the melting point of Ci3NC crystal. It is clear from the DTA curve that there is no phase transition before melting. The sharpness of the peak demonstrated good crystallinity and purity of the sample, which is in tune with the results obtained from HRXRD. The TG curve of this sample indicates that the sample was stable up to 220 °C. The exothermic peak of the DTA at 286.00 °C, corresponding to the weight loss in the TG curve, indicated that the weight loss was due to the degradation and evaporation of the sample. Melting point of Ci3NC was determined by the open capillary method and was uncorrected. It has a quite high melting point of 138.3 °C, which was the same as measured by thermal analysis.

3.3. UV–vis–NIR absorption spectrum

The UV–vis–NIR spectrum of the crystal is depicted in Fig. 5. The cutoff wavelength for this crystal was found to be 424 nm. Above this range no absorption peaks were present until the IR spectral region. The maximum absorption was assigned for the n–π^* transition and may be attributed to the excitation of C=O group. Only n–π^* electronic transition is possible since the C=O group of Ci3NC absorbs UV light and promotes excitation of electrons from one of the unshared pair n (from non-bonding orbital) to anti-bonding π^* orbital in the molecules [17,18]. The wide transparency range will be helpful for these crystals to be used for NLO applications.

3.4. Second harmonic generation (SHG) efficiency

The second harmonic generation efficiency for Ci3NC was found to be 7 times that of urea crystals of identical particle size. The SHG signal provides a highly sensitive and definitive test for the absence of a center of symmetry in the compound. The Ci3NC crystal can be considered as a donor–π–acceptor–π–acceptor system, where charge transfer takes place from donor to acceptor group.The presence of donor–acceptor groups, charge transfer axis, parallel head to tail arrangement in crystal packing, and the number of intermolecular bonding enabled Ci3NC to have higher SHG efficiency than urea [11].

3.5. Nonlinear optical studies

The NLO studies were performed for the sample Ci3NC (in solution form) with linear transmittance of ~90% at 870 nm and 900 nm. We measured NLO coefficients using an optical chopper with frequency range from 100 Hz to 4 kHz. We recorded the data by placing the chopper in front of the lens at 500 Hz and 1 kHz with the beam diameter of 3 mm at the wavelength of 900 nm. Fig. 6 (a) and (b) shows the closed aperture and open aperture data of Ci3NC at 80 MHz at 900 nm. From the closed aperture data (recorded with a peak intensity of ~0.034 GW/cm^2) the value of n_2 was obtained as $\sim10^{-14}$ cm^2 W^{-1}. From the open aperture data we obtained 3PA coefficient (γ) of $\sim10^{-15}$ cm^3 W^{-2} with a peak intensity of ~0.20 GW/cm^2. Fig. 6(c) and (d) depicts the Z-scan data obtained for the sample at 870 nm. The values of γ and n_2 obtained from the fits were $\sim10^{-15}$ cm^3 W^{-2} and $\sim10^{-13}$ cm^2 W^{-1}, respectively. Fig. 7(a) and (b) shows the closed aperture and open aperture data of Ci3NC obtained using a 1 kHz chopper at 900 nm. In this case, we attained 2PA coefficient of β of $\sim10^{-8}$ cm W^{-1} for data recorded with a peak intensity of ~0.32 GW/cm^2 at 1 kHz. The values of n_2 were $\sim10^{-14}$ cm^2 W^{-1} obtained from the fit to the data recorded with peak intensity of ~0.034 GW/cm^2. Fig. 7(c) and (d) illustrates the Z-scan data (500 Hz) obtained at 870 nm. We obtained 2PA coefficient of β with a magnitude of 10^{-9} cm W^{-1} for data recorded with a peak intensity of ~0.33 GW/cm^2. The values of n_2 were $\sim10^{-13}$ cm^2 W^{-1} obtained from the fit to the data recorded with peak intensity of ~0.034 GW/cm^2. All NLO coefficients were estimated with 15% uncertainty arising from errors in beam waist measurements and calibration of neutral density filters. Since the experiments were performed with high repetition rate pulses we expect strong thermal contribution (through heating of the sample) to the observed large NLO nonlinear coefficients. With 80 MHz excitation there could possibly be contribution from other excited states leading to 3PA. Even though the pulses were chopped with 1 kHz and 500 Hz frequency, the obtained pulses are not truly kHz pulses since we get bunches of pulses at kHz repetition rate. Further experiments are required to identify the reasons for observing 2PA at lower repetition rates. However, the NLO coefficients obtained represent one of the largest reported in recent literature [22–25]. The contribution from solvent to the measured NLO coefficients was found to be negligible.

The results in Table 1 exhibit that Ci3NC possesses large third-order NLO properties, which can be explained from its molecular structure. Ci3NC is designed based on the scheme donor–acceptor–acceptor group [22]. The large third-order NLO properties arise in Ci3NC due to the strong delocalization of π-electrons. Generally, in π-conjugated molecules, the charge cloud formed by conjugated π-electrons has the capability of being strongly deformed under the effect of an external optical field. The nitro group attached to phenyl ring on one side of the carbonyl group acts as an acceptor due to inductive effect [23]. At the center, the presence of oxygen in the carbonyl group (C=O) is more electronegative. Hence, it acts as an acceptor. On the other side of the carbonyl group, the phenyl ring acts as a donor. Thus, the charge transfer takes place from one end to the center and the other end of the molecule leading to the large nonlinearity. Our future

studies will incorporate NLO measurements using truly 1 kHz, fs pulses to estimate the electronic contribution to the nonlinearity.

4. Conclusions

Single crystals of Ci3NC exhibit both second and third order nonlinear optical properties. The powder SHG value of the crystal is 7 times that of urea. The crystal is transparent for the fundamental and SHG of Nd:YAG laser ($\lambda = 1064$ nm) and is stable up to 220 °C without any phase transition. The diffraction curve of the high resolution XRD results confirms that the crystalline perfection is reasonably good. We observed 3PA as dominant nonlinear absorption process with 80 MHz excitation while 2PA was observed when the data was collected with a chopper with lower repetition rate (1 kHz and 500 Hz data).

References

[1] Sutherland RL. Hand book of nonlinear optics. 2nd ed.. . New York: Dekker; 1996.
[2] Prasad PN, Williams DJ. Introduction to nonlinear optical effects in organic molecules and polymers. New York: John Wiley & Sons; 1991.
[3] Chemla DS, Zyss J. Nonlinear optical properties of organic molecules and crystals. Orlando: Academic Press; 1987.
[4] Bailey RT, Bourhill G, Cruickshank FR, Pugh D, Sherwood JN, Simpson GS. The linear and nonlinear optical properties of the organic nonlinear material 4-nitro-4′-methylbenzylidene aniline. J Appl Phys 1993;73:1591–7.
[5] Cole JM. Organic materials for non-linear optics: advances in relating structure to function. R Soc Philos Trans 2003;A 361:2751–70.
[6] Bing Gu, Wei Ji, Xiao-Qin Huang, Patil PS, Dharmaprakash SM. Nonlinear optical properties of 2,4,5-trimethoxy-4′-nitrochalcone: observation of two-photon-induced excited-state nonlinearities. Opt Express 2009;17:1126–35.
[7] Rodenberger DC, Heflin JR, Garrto AF. Excited-state enhancement of optical nonlinearities in linear conjugated molecules. Nature 1992;359:309–11.
[8] D'Silva ED, Krishna Podagatlapalli G, Venugopal Rao S, Dharmaprakash SM. Study on third-order nonlinear optical properties of 4-methylsulfanyl chalcone derivatives using pico second pulses. Mater Res Bull 2012;47:3552–7.
[9] Chen Jing wei, Wang Xinqiang, Quan Ren, Patil PS, Tingbin Li, Hongliang Yang, et al. Investigation of third-order nonlinear optical properties of NNDC-doped PMMA thin films by Z-scan technique. Appl Phys A 2011;105:723–31.
[10] Patil PS, Bhumannavar VM, Bannur MS, Kulkarni Harish N, Bhagavannarayana G. Second harmonic generation in some donor–acceptor substituted chalcone derivatives. J Cryst Process Technol 2013;3:108–17.
[11] Patil PS, Teh Jeannie Bee-Jan, Fun Hoong-Kun, Razak Ibrahim Abdul, Dharmaprakash SM. (2E,4E)-1-(3-nitrophenyl)-5-phenylpenta-2,4-dien-1-one. Acta Crystallogr Sect E 2007;63:o2122–3.
[12] Tunyagi A, Ulex M, Betzler K. Non-collinear optical frequency doubling in strontium barium niobate. Phys Rev Lett 2003;90:243901.
[13] Lal Krishan, Bhagavannarayana G. A high-resolution diffuse X-ray scattering study of defects in dislocation-free silicon crystals grown by the float-zone method and comparison with Czochralski-grown crystals. J Appl Crystallogr 1989;22:209–15.
[14] Kurtz SK, Perry TT. A powder technique for the evaluation of nonlinear optical materials. J Appl Phys 1968;39:3798–813.
[15] Bahae MS, Said AA, Wei TH, Hagan DJ, Van Stryland EW. Sensitive measurement of optical nonlinearities using a single beam. IEEE J Quantum Electron 1990;26:760–9.
[16] Bhagavannarayana G, Ananthamurthy RV, Budakoti GC, Kumar B, Bartwal KS. A study of the effect of annealing on Fe-doped LiNbO3 by HRXRD, XRT and FT-IR. J Appl Crystallogr 2005;38:768–71.
[17] Shettigar V, Patil PS, Naveen S, Dharmaprakash SM, Sridhar MA, Shashidhara Prasad J. Crystal growth and characterization of new nonlinear optical chalcone derivative:1-(4-methoxyphenyl)-3-(3,4-dimethoxyphenyl)-2-pro-pen-1-one. J Cryst Growth 2006;295:44–9.
[18] D'silva ED, Narayan Rao D, Reji Philip, Ray Butcher J, Rajnikant, Dharmaprakash SM. Second harmonic chalcone crystal: synthesis, growth and characterization. Phys B: Condens Matter 2011;406:2206–10.
[19] Swain D, Anusha PT, Prashant TS, Tewari SP, Sarma T, Panda PK, et al. Ultrafast excited state dynamics and dispersion studies of nonlinear optical properties in dinaphthoporphycenes. Appl Phys Lett 2012;100:141109.
[20] Anusha PT, Reeta PS, Giribabu L, Tewari SP, Venugopal Rao S. Mater Lett 2010;64:1915–7.
[21] Hamad S, Tewari SP, Giribabu L, Venugopal Rao S. Picosecond and femtosecond optical nonlinearities of novel corroles. J Porphyr Phthalocyanines 2012;16:140–8.
[22] Fitilis I, Fakis M, Polyzos I, Giannetas B, Persephonis P, Vellis P, et al. A two-photon absorption study of fluorene and carbazole derivatives. The role of the central core and the solvent polarity. Chem Phys Lett 2007;447:300–4.
[23] Gu Bing, Ji Wei, Patil PS, Dharmaprakash SM. Ultrafast optical nonlinearities and figures of merit in acceptor-substituted 3,4,5-trimethoxychalcone derivatives: structure–property relationships. J Appl Phys 2008;103:103511–6.
[24] Shettigar S, Poornesh P, Umesh G, Sarojini BK, Narayana B, Prakash Kamath K. Investigation of third-order nonlinear optical properties of conjugated benzodioxal derivatives. Opt Laser Technol 2010;42:1162–6.
[25] Kiran AJ, Nooji SR, Udayakumar D, Chandrasekharan K, Kalluraya B, Philip R, et al. Nonlinear optical properties of p-(N,N-dimethylamino)dibenzylideneacetone doped polymer. Mater Res Bull 2008;43:707–13.